Iraqi Journal of Physics, 2023 *Vol. 21 No. 3, PP. 24-32*

https://doi.org/10.30723/ijp.v21i3.1124 *P-ISSN: 2070-4003*
E-ISSN: 2664-5548

Study the Electronic and Spectroscopic Characteristics of p-n Heterojunction Hybrid ($Sn_{10}O_{16}/C_{24}O_6$) via Density Functional Theory (DFT)

Shaima K. Abdulradha[1a]*, Mohammed T. Hussein[1b] and Mudar Ahmed Abdulsattar[2c]
[1]*Department of Physics, College of Science, University of Baghdad, Baghdad, Iraq*
[2]*Ministry of Science and Technology, Baghdad, Iraq*
[b]E-mail: mohammedtake@gmail.com, [c]E-mail: mudarahmed3@yahoo.com
[a*]Corresponding author: shaimaa.khayoon1104a@sc.uobaghdad.edu.iq

Abstract

The electronic characteristics, including the density of state and bond length in addition to the spectroscopic properties such as IR spectrum and Raman scattering, as a function of the frequency of $Sn_{10}O_{16}$, $C_{24}O_6$, and hybrid junction ($Sn_{10}O_{16}/C_{24}O_6$) were studied. The methodology uses DFT for all electron levels with hybrid function B3-LYP (Becke level, 3-parameters, Lee–Yang-Parr), with 6-311G (p,d) basis set and (Stuttgart/Dresden) SDD basis set, using Gaussian 09 theoretical calculations. The geometrical structures were calculated by Gaussian view 05 as a supplementary program. The band gap was calculated and compared to the measured values. The density of state of the hybrid junction ($Sn_{10}O_{16}/C_{24}O_6$) increased because of the increased number of degeneracy states. Theoretical values of bonds for C=C, C=O, and Sn-O are equal to 1.33, 1.20 and 2.27 Å respectively, these bonds values are in good agreement with experimental values bond length of (1.34 for the C=C bond, 1.23 for the C=O bond, and 2.3 for the Sn-O bond) Å. The spectroscopic properties such as IR spectra have shown a peak which is comparable to longitudinal modes of GO and tin dioxide SnO_2 at (1582 and 690) cm^{-1}, respectively.

Article Info.

Keywords:
Reduced graphene oxide (rGO), Tin dioxide (SnO_2), p-n Heterojunction hybrid, DFT, Electronic properties.

Article history:
Received: Apr.17,2023
Revised: Jul. 27, 2023
Accepted: Aug.03,2023
Published: Sep.01,2023

1. Introduction

Materials that eliminate oxygen-containing functional groups from the surface of graphene oxide may be used to activate graphene oxide. Graphene oxide can then be used in various applications. One of the substances that can be used in the process of stripping graphene oxide's surface of its oxygen layer is hydrazine [1-4]. The produced substance is then known as reduced graphene oxide (rGO), which is a p-type semiconductor [5, 6]. RGO combines the properties of graphene and graphene oxide. Although it is hydrophobic, it can spread in water and organic solvents. Because it contains few oxygen groups, rGO is similarly insoluble in polar solvents. It has good electrical conductivity [7-10].

Tin dioxide (SnO_2) is an n- type semiconductor; it is one example of transparent conductive oxides (TCO). It has high transmittance in the ultraviolet-visible region [11-14]. Tin dioxide is a wide band energy gap (3.7 eV) semiconductor [15-20]. It is white in color and has a tetragonal crystalline structure [21]. Tin dioxide (SnO_2) is one of the most used materials for gas sensors; it is used to detect hydrocarbons [22-25]. SnO_2 nanoparticles are anticipated to be superior in their sensitivity to gases than bulk material because of larger surface area. SnO_2 pyramids are experimentally found on SnO_2 surfaces as a result of surface reconstruction [26, 27]. These pyramids are found stable and able to explain the experimental findings of Indium doped SnO_2 nanoclusters [27]. The electronic characteristics of Coronen (C_{24}) and rGO $C_{24}O_X$, where x = 1–5, as well as their spectroscopic properties, such as infrared and Raman spectra, force constants, and reduced masses, were examined using the Density Functional Theory

(DFT) at hybrid function B3LYP and 6-311G** basis sets. The calculated energy gaps and spectroscopic properties are in good agreement with the experiment results [28]. Density Functional Theory (DFT) with a B3LYP (Becke 3-parameter, Lee–Yang-Parr) level at 6-311G** basis sets for light atoms such as N and O as well as SDD (Stuttgart/Dresden) basis sets for heavy atoms like Sn were used in conjunction with the Gaussian 09W software to investigate the reaction of tin dioxide nanocrystals and NO_2 at temperatures ranging from 273 to 373 degrees Celsius. The analysis was carried out at different temperatures. It is possible to calculate the Gibbs energy, as well as enthalpy and entropy [29]. The objective of this research is to study the electronic and spectral characteristics of reduced graphene oxide ($C_{24}O_6$) and tin dioxide ($Sn_{10}O_{16}$), as well as a comparison with the interaction properties of ($C_{24}O_6/Sn_{10}O_{16}$) hybrid junction using the DFT approach. The theoretical results were compared with the experimental results for the compounds used in this paper.

2. Theory

In this study, the structural and vibrational properties were determined using the engineering optimization method. Using the computer program Gaussian 09 and theoretical estimates, the properties and nanostructure of graphene oxide and tin dioxide were predicted. DFT and GGA (Generalized Gradient Approximation) were included as a term in the equation for the hybrid function (B3LYP), which were applied with 6-311G (p,d) for light atoms ($C_{24}O_6$) and SDD for heavy atoms ($Sn_{10}O_{16}$), where the scaling factor was 0.967 and 0.960 to correct for vibration frequencies [30-34]. The geometrical structures were calculated by Gaussian 05 view as a complementary program [35, 36]. Fig. 1 shows the geometries of (a) $Sn_{10}O_{16}$, (b) $C_{24}O_6$ and (c) $Sn_{10}O_{16}/C_{24}O_6$. It is impossible to simulate a very large number of atoms using more than 100 atoms in the Gaussian 09 program because of the long-needed computer time. As a result, a common practice and many successful simulations of rGO are performed using small rGO clusters as was done by Pal et al. [37]; the experimental work showed that rGO is similar to the structure (a) in Fig. 1 [38]. The SnO_2 cluster is repelled as a result of performing self-consistent field calculations of the present density functional theory. As a result, the attachment is made between one of the carbon atoms at the edge of rGO and one Sn atom at the edge of SnO_2, as seen in Fig. 1 (c).

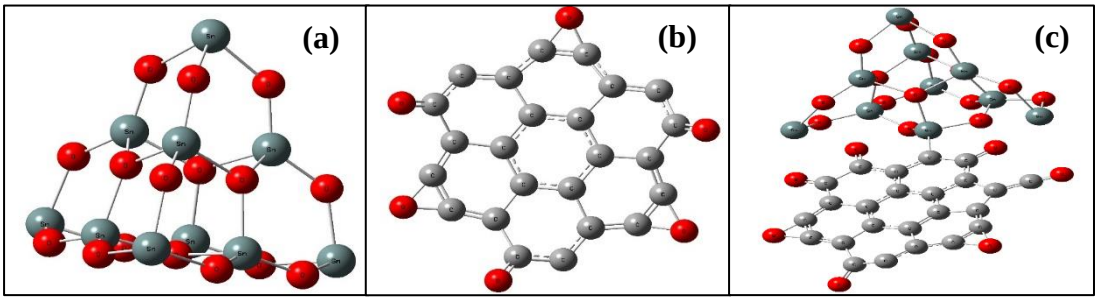

Figure 1: Shows geometric for (a) $Sn_{10}O_{16}$, (b) $C_{24}O_6$ and (c) $Sn_{10}O_{16}/C_{24}O_6$.

3. Results and Discussion

3.1. Electronic Properties

The density of states (DOS) is a measure of the number of energy states per unit volume per unit energy range. It provides information about the distribution of available energy states within a material. When determining the electronic characteristics of solids, one of the most important factors is the distribution of energy between the

electrons in the valence band (V.B.) and the conduction band (C.B.). The energy gap (E_g) calculation is found by the following equation [39]:

$$E_g = | First_{(LUMO)} - Last_{(HOMO)} | \quad (1)$$

The change in the HOMO (V.B.) and LUMO (C.B.) states can be represented by the density of the state. Fig. 2 shows the density of states for $Sn_{10}O_{16}$, $C_{24}O_6$, and $Sn_{10}O_{16}/C_{24}O_6$ according to the energy levels. It can see that the energy gap for $Sn_{10}O_{16}$ is (3.8 eV) compared to the experimental value of (3.7 eV) for SnO_2 [15-20], while the energy gap of $C_{24}O_6$ is equal to (1.33) eV compared to the experimental value of reduced graphene oxide is (1-2.2 eV) [40-42].

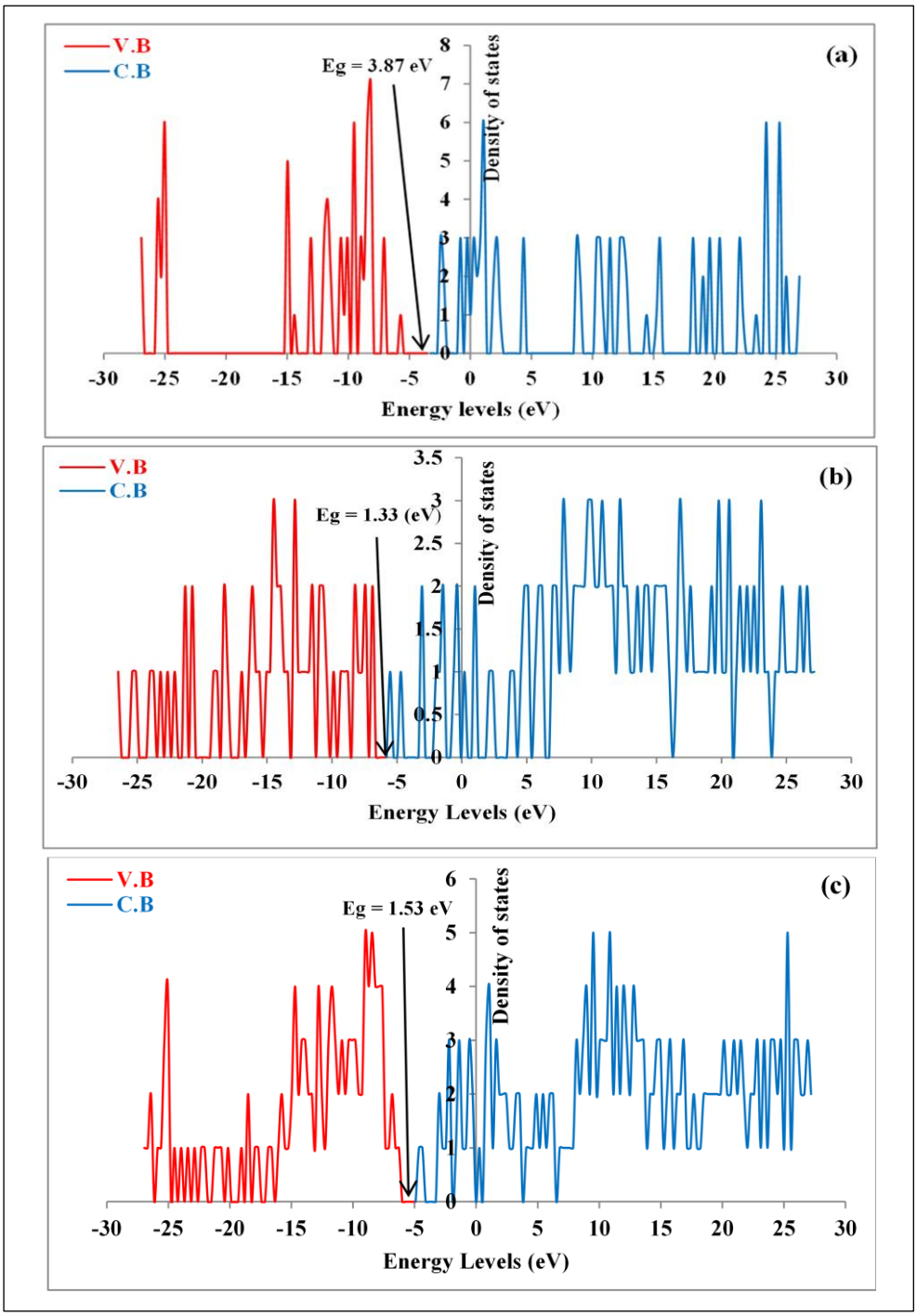

Figure 2: Density of states for (a) $Sn_{10}O_{16}$, (b) $C_{24}O_6$ and (c) $Sn_{10}O_{16}/C_{24}O_6$ based on energy levels.

While the energy gap of the whole structure $Sn_{10}O_{16}/C_{24}O_6$ is equal to (1.53) eV, this decrease is because of the ease of movement of the electrons due to the decrease in the resistance and increase in the conductivity, as shown in Fig. 2.

Fig. 3 shows the bond densities of $Sn_{10}O_{16}$, $C_{24}O_6$, and $Sn_{10}O_{16}/C_{24}O_6$ hybrid junction. The bonding between $Sn_{10}O_{16}$ and $C_{24}O_6$ is formed since the two molecules are brought together as shown in Fig 3. The contact region between p-n junction is called the space charge region, which is of vital importance in p-n junctions. There are three kinds of bonds C=C, C=O, and Sn-O. Sn-O bonds are the strongest, followed by C=C and C=O bonds in terms of bond length. The bond lengths are (1.33, 1.20, and 2.27) Å, respectively. These length bond values are in good agreement with experimental values bond length of 1.34 Å for the C=C bond, 1.23 Å for the C=O bond and 2.3Å for the Sn-O bond [43-46]. The theoretical results also showed their agreement with the experimental.

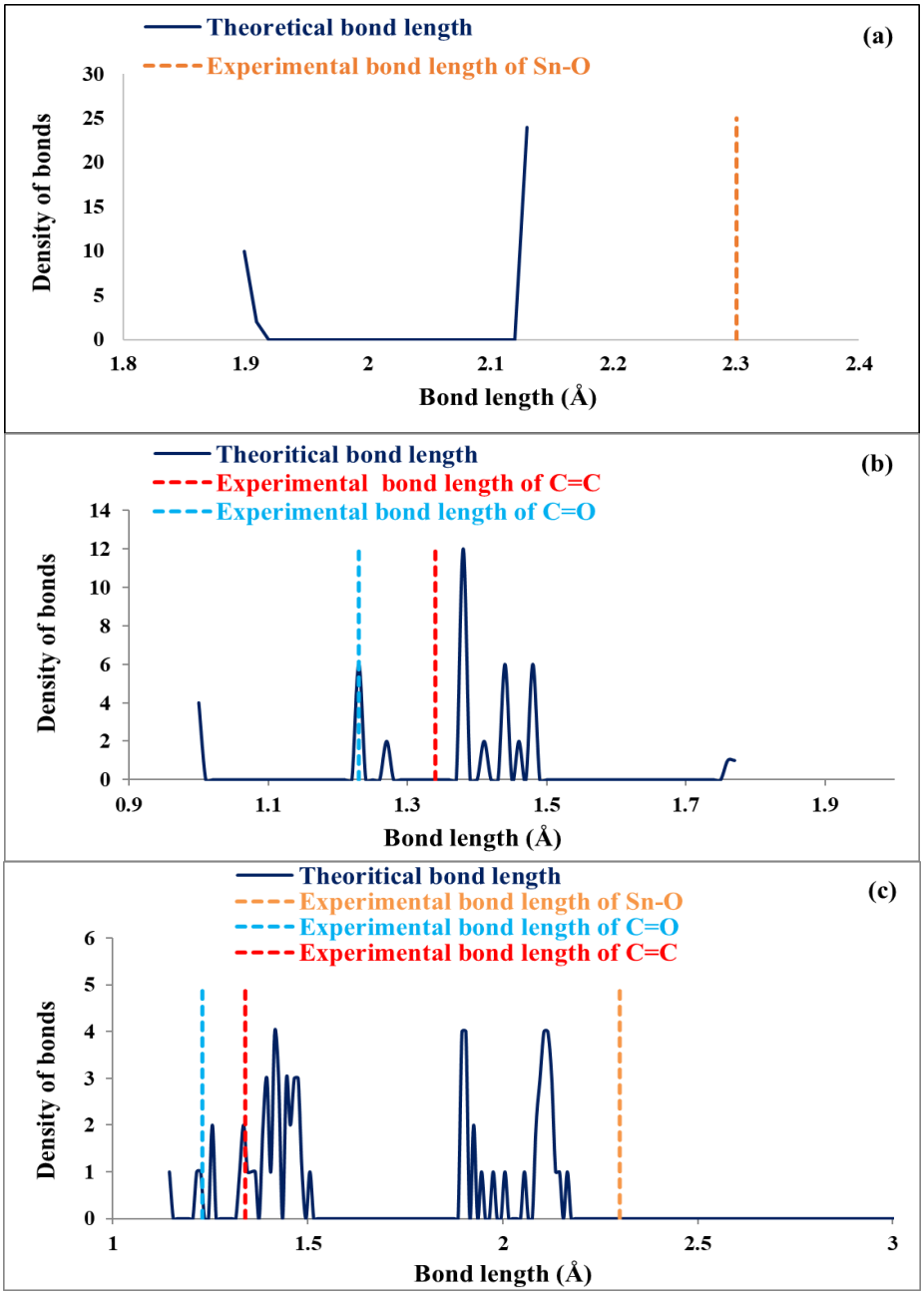

Figure 3: Bonds Density for (a) $Sn_{10}O_{16}$, (b) $C_{24}O_6$ and (c) $Sn_{10}O_{16}/C_{24}O_6$ based on bond length.

3.2. Spectroscopy Characteristic

3.2.1. IR and Raman spectrum

Fig. 4 and Fig.5 display IR spectra and Raman spectra for (a) $Sn_{10}O_{16}$, (b) $C_{24}O_6$, and (c) $Sn_{10}O_{16}/C_{24}O_6$ hybrid junction as a function of frequency. There are three different vibrational frequency bands for IR spectra of $Sn_{10}O_{16}$, $C_{24}O_6$ and $Sn_{10}O_{16}/C_{24}O_6$ hybrid junction at (755.2, 1688 and 2238) cm^{-1}, respectively. The shift of the highest peak towards the high-frequency region in the IR spectrum during the interaction between ($Sn_{10}O_{16}/C_{24}O_6$) junction indicates a change in the molecular vibrations and bonding environment of the material. When these materials interact or form a junction, their molecular structures and bonding arrangements are affected, leading to changes in their vibrational modes. Similar bands were shown in Raman spectra but with lower intensity. These theoretical frequencies are comparable with the experimental values of longitudinal modes of (SnO_2 and GO, which were (690 and 1582) cm^{-1}, respectively [47-50].

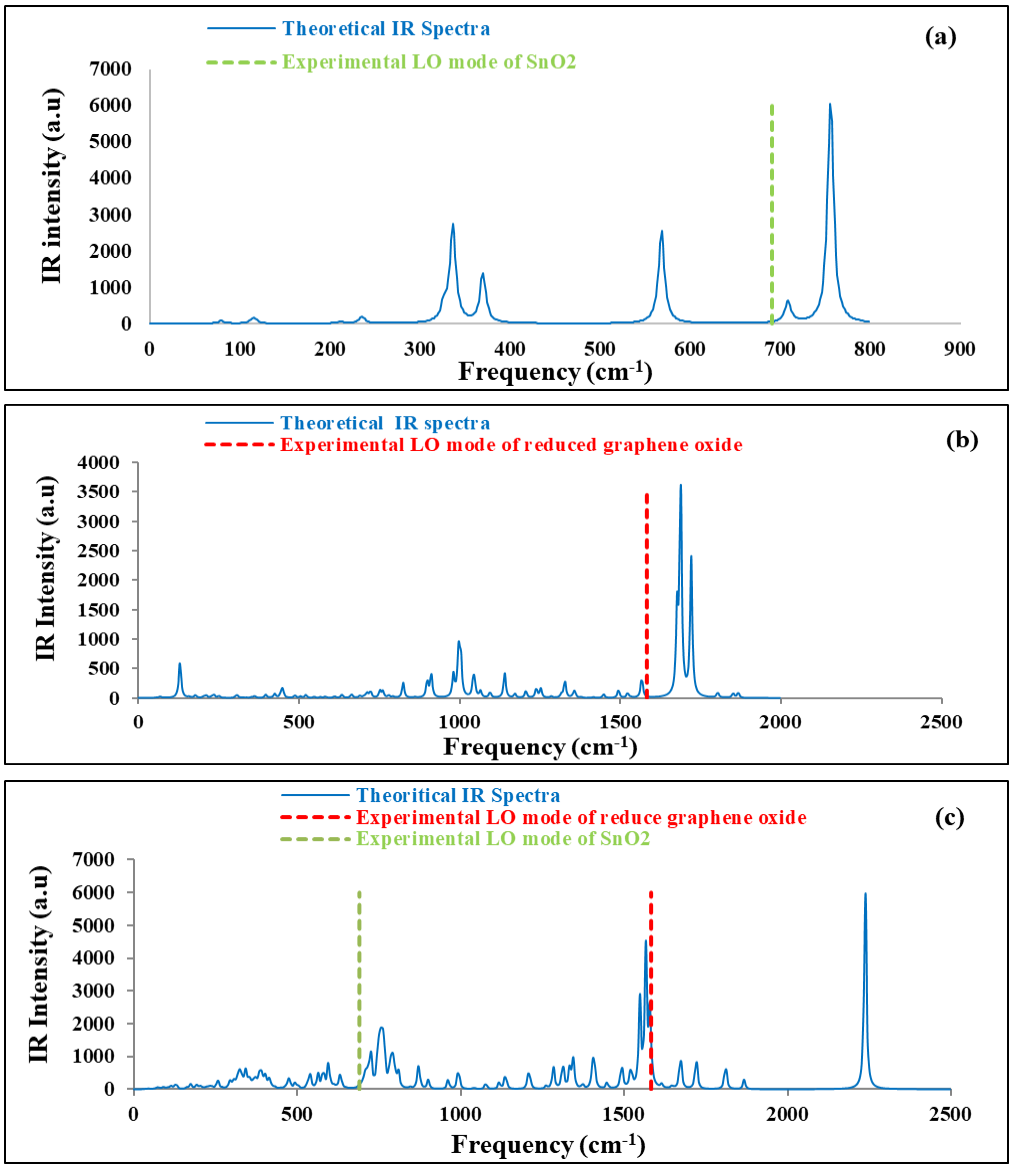

Figure 4: The infrared spectra of (a) $Sn_{10}O_{16}$, (b) $C_{24}O_6$ and (c) $Sn_{10}O_{16}/C_{24}O_6$ as a function of frequency.

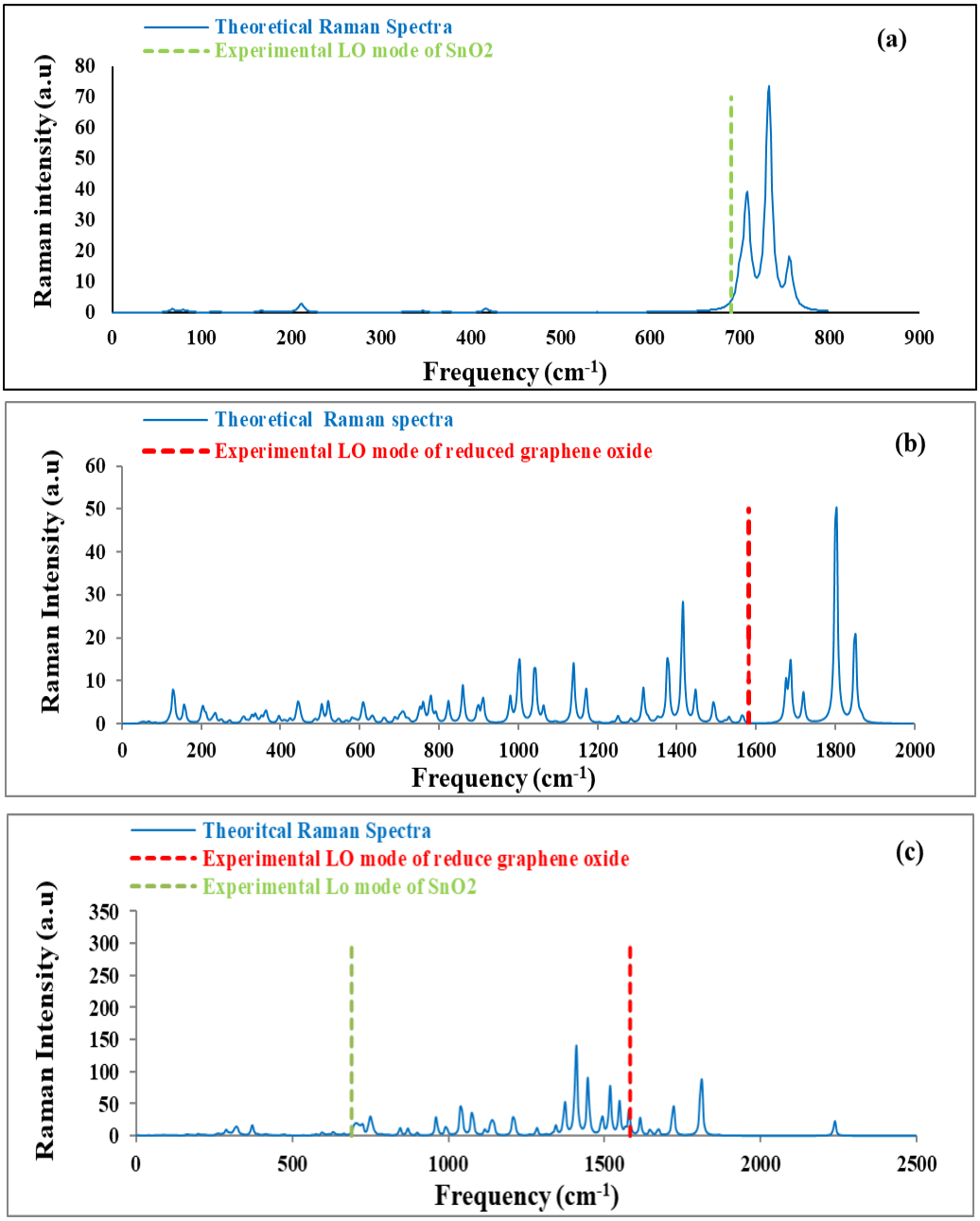

Figure 5: The Raman spectra for (a) $Sn_{10}O_{16}$, (b) $C_{24}O_6$, and (c) $Sn_{10}O_{16}$/ $C_{24}O_6$ as a function of frequency.

4. Conclusions

As a result of research on the electronic and spectral properties of hybrid junction ($Sn_{10}O_{16}/C_{24}O_6$), the energy band gap decreased compared with the experimental value indicating a decrease in the resistance and an increase in the conductivity. The final calculated gap of the rGO/SnO_2 hybrid was (1.53) eV, with the HOMO and LUMO energy levels moved to be higher than that of rGO. There is a distribution of bond lengths, with the highest peaks corresponding to bulk values. There are three types of bonds: C=C, C=O, and Sn-O. It was found that the bond length values are in good agreement with the experimental values. The theoretical value agrees with the experimental value of longitudinal modes of graphene oxide (GO) and tin dioxide (SnO_2) at (1582 and 690) cm^{-1}, respectively.

Acknowledgements

The authors would like to thank University of Baghdad, Collage of Science, Department of Physics.

Conflict of interest

Authors declare that they have no conflict of interest.

References

1. Z. Wang, Z. Jia, Q. Li, X. Zhang, W. Sun, J. Sun, B. Liu, and B. Ha, J. Coll. Inter. Sci. **537**, 228 (2019).
2. X. Xu, J. Zeng, Y. Wu, Q. Wang, S. Wu, and H. Gu, Separations **9**, 401 (2022).
3. F. El-Hossary, A. Ghitas, A. Abd El-Rahman, M. A. Shahat, and M. H. Fawey, Vacuum **188**, 110158 (2021).
4. E. F. Joel and G. Lujanienė, Environments **9**, 153 (2022).
5. S. Drewniak, Ł. Drewniak, and T. Pustelny, Sensors **22**, 5316 (2022).
6. D.-T. Phan and G.-S. Chung, J. Phys. Chem. Sol. **74**, 1509 (2013).
7. R. Hajian, K. Fung, P. P. Chou, S. Wang, S. Balderston, and K. Aran, Mater. Matt. **14**, 1 (2019).
8. Y. Xiao, Y. X. Pang, Y. Yan, P. Qian, H. Zhao, S. Manickam, T. Wu, and C. H. Pang, Advan. Sci. **10**, 2205292 (2023).
9. S. Wu, X. Wang, Z. Li, S. Zhang, and F. Xing, Micromachines **11**, 1059 (2020).
10. A. M. Pandele, M. Oprea, A. A. Dutu, F. Miculescu, and S. I. Voicu, Polymers **14**, 148 (2021).
11. J. E. House and K. A. House, *Descriptive Inorganic Chemistry*. 2nd Ed. (Burlington, USA, Elesevier, 2015).
12. O. E. Oladigbo, O. Adedokun, and Y. K. Sanusi, Int. J. Eng. Sci. Appl. **2**, 88 (2018).
13. A. Marikuts, M. Rumyantseva, and A. Gaskov, Proced. Eng. **168**, 1082 (2016).
14. H. K. Saglam, M. Masat, and M. Ertugrul, Int. J. Innov. Res. Rev. **5**, 69 (2021).
15. S. Baco, A. Chik, and F. M. Yassin, J. Sci. Tech. **4**, 61 (2012).
16. S. Ebrahimiasl, W. M. Z. W. Yunus, A. Kassim, and Z. Zainal, Sensors **11**, 9207 (2011).
17. S. Mohana Priya, A. Geetha, and K. Ramamurthi, J. Sol-Gel Sci. Tech. **78**, 365 (2016).
18. G. K. Dalapati, H. Sharma, A. Guchhait, N. Chakrabarty, P. Bamola, Q. Liu, G. Saianand, A. M. S. Krishna, S. Mukhopadhyay, and A. Dey, J. Mat. Chem. A **9**, 16621 (2021).
19. O. Filonenko, A. Grebenyuk, and V. Lobanov, Chem., Phys. Tech. Surf. **12**, 283 (2021).
20. S. M. Yakout, Opt. Mat. **116**, 111077 (2021).
21. T. Kim, D. Lee, J. Lee, D. Choo, M. Jung, and Y. Yoon, J. Appl. Phys. **90**, 175 (2001).
22. P. T. Hernández, S. Hailes, and I. Parkin, Sens. Actuat. B: Chem. **242**, 1281 (2017).
23. S. Mala, H. Lalithamba, N. Gowda, K. Manoja, R. Pavankumar, and T. Kishore, in International Conference on Smart Systems for applications in Electrical Sciences, IEEE, 2023, p. 1.
24. Q. Zhang, Q. Zhou, Z. Lu, Z. Wei, L. Xu, and Y. Gui, Front. Chem. **6**, 364 (2018).
25. M. A. Abdulsattar, D. A. Nassrullah, and Z. T. Abdulhamied, J. Advan. Pharm. Edu. Res. **9**, 119 (2019).
26. S. Das, D.-Y. Kim, C.-M. Choi, and Y. Hahn, J. Crys. Gro. **314**, 171 (2011).

27. M. A. Abdulsattar, S. S. Batros, and A. J. Addie, Superlatt. Microstruc. **100**, 342 (2016).
28. M. A. Hadi and M. T. Hussein, Iraqi J. Sci. **64**, 157 (2023).
29. N. F. Jafer and M. T. Hussein, Int. J. Nanosci. **21**, 2250006 (2022).
30. F. Hasan and M. Hussein, Mat. Today: Proce. **42**, 2638 (2021).
31. M. Hussein, T. Fayad, and M. Abdulsattar, Chalcog. Lett. **16**, 557 (2019).
32. E. Zins, M. Guinet, D. Rodriguez, and S. Payan, J. Quan. Spect. Rad. Tran. **283**, 108141 (2022).
33. M. A. Abdulsattar, Karbala Int. J. Mod. Sci. **6**, 205 (2020).
34. N. Kerru, L. Gummidi, S. V. Bhaskaruni, S. N. Maddila, P. Singh, and S. B. Jonnalagadda, Sci. Rep. **9**, 19280 (2019).
35. M. A. Matin, M. M. Islam, T. Bredow, and M. A. Aziz, Advan. Chem. Eng. Sci. **7**, 137 (2017).
36. M. T. Hussein and H. A. Thjeel, in Journal of Physics: Conference Series, IOP Publishing, 2019, p. 012015.
37. P. Pal, A. Yadav, P. S. Chauhan, P. K. Parida, and A. Gupta, Sens. Int. **2**, 100072 (2021).
38. W. Zhang, X. Xiao, X. Zeng, Y. Li, L. Zheng, and C. Wan, J. All. Comp. **685**, 774 (2016).
39. A. H. Taha, American J. Conden. Mat. Phys. **4**, 63 (2014).
40. Abid, P. Sehrawat, S. Islam, P. Mishra, and S. Ahmad, Sci. Rep. **8**, 3537 (2018).
41. E. Mattson, J. Johns, K. Pande, R. Bosch, S. Cui, M. Gajdardziska-Josifovska, M. Weinert, J. Chen, M. Hersam, and C. Hirschmugl, J. Phys. Chem. Lett. **5**, 212 (2014).
42. H. Liang, AIP Advan. **4**, 107131 (2014).
43. J. D. Roberts and M. C. Caserio, *Basic Principles of Organic Chemistry*. (New York; Amsterdam, WA Benjamin, Inc., 1977).
44. Y. Salem, C. Abdelkader, and H. Fodil, Chinese J. Struct. Chem. **32**, 1544 (2013).
45. T. Sivaranajani, T. Jayavarthanan, S. Suresh, C. Biju, A. Jayanthi, L. Sangeetha, C. Saveetha, A. a. P. Frit, and M. Muruganandam, Chem. Phys. Imp. **6**, 100200 (2023).
46. Y. Chen, H. Qin, Y. Cao, H. Zhang, and J. Hu, Sensors **18**, 3425 (2018).
47. Y. Shen, S. Yang, P. Zhou, Q. Sun, P. Wang, L. Wan, J. Li, L. Chen, X. Wang, and S. Ding, Carbon **62**, 157 (2013).
48. S. Sambasivam and I. M. Obaidat, Mat. Today: Proc. **28**, 587 (2020).
49. J.-B. Wu, M.-L. Lin, X. Cong, H.-N. Liu, and P.-H. Tan, Chem. Soci. Rev. **47**, 1822 (2018).
50. H. Alghamdi, O. Z. Farinre, M. L. Kelley, A. J. Biacchi, D. Saha, T. Adel, K. Siebein, A. R. H. Walker, C. A. Hacker, and A. F. Rigosi, Data **8**, 37 (2023).

دراسة الخصائص الإلكترونية والطيفية للهجين (p-n) ($Sn_{10}O_{16}$ / $C_{24}O_6$) باستخدام نظرية دالية الكثافة (DFT)

شيماء خيون عبدالرضا [1] و محمد تقي حسين[1] و مضر احمد عبدالستار[2]
[1]قسم الفيزياء، كلية العلوم، جامعة بغداد، العراق
[2]وزارة العلوم والتكنولوجيا،بغداد، العراق

الخلاصة

تمت دراسة الخواص الالكترونية المتضمنه كثافة الحالة وطول الاصرة بالإضافة الى الخصائص الطيفية مثل طيف الاشعة تحت الحمراء واستطارة رامان كدالة للتردد ل ($Sn_{10}O_{16}$, $C_{24}O_6$) ودالة الهجين ($Sn_{10}O_{16}$/ $C_{24}O_6$). تستخدم المنهجية الحالية لكل الالكترونات نظرية دالية الكثافة DFT مع الداله الهجينه B3LYP ومجموعه الاساس (p, d) 6-311G وSDD باستخدام Gaussian 09 للحسابات النظرية. تم حساب التراكيب الهندسية باستخدام برنامج تكميلي Gaussian view 05. تم حساب فجوة الطاقة ومقارنتها بفجوة الطاقة المحسوبه. تزداد كثافة الحالة عند الهجين ($Sn_{10}O_{16}$ / $C_{24}O_6$) بسبب زيادة عدد حالات الانحلال. القيم النظرية لكثافة الروابط لـ C = C، C = O وSn-O تساوي (1.33، 1.20 و 2.27) انكستروم على التوالي وتتفق قيم هذه الروابط جيدًا مع القيم التجريبية وطول الرابطه (1.34 للرابطة C = C، 1.23للرابطة C = O و 2.3 للرابطة Sn-O) انكستروم. الخصائص الطيفية مثل الأشعة تحت الحمراء يمكن مقارنتها بالأنماط الطولية للكرافين اوكساید GO وثاني أوكسيد القصدير(SnO_2) عند (1582 و 690) سم$^{-1}$ على التوالي.

الكلمات المفتاحية: اوكسيد الكرافين المختزل، ثاني اوكسيد القصدير،هجين غير متجانس p-n، نظرية دالية الكثافة، الخواص الالكترونية.